UDK 621.93.026.4:546.261
Original scientific article/Izvirni znanstveni članek

ISSN 1580-2949
Mater. Tehnol.

FRACTURE ANALYSIS OF CEMENTED-CARBIDE INSERTS FOR THE DRY CUTTING OF REPEN LIMESTONE

ANALIZA PORUŠITVE REZALNIH PLOŠČIC IZ KARBIDNE TRDINE PRI SUHEM REZANJU REPENSKEGA APNENCA

Jože Kortnik*, Boštjan Markoli, Matej Zupančič, Adam Zaky, Iztok Naglič

University of Ljubljana, Faculty of Natural Sciences and Engineering, Aškerčeva 12, 1000 Ljubljana, Slovenia

Prejem rokopisa – received: 2025-01-13; sprejem za objavo – accepted for publication: 2025-02-17

doi:10.17222/mit.2024.1372

This paper presents the results of an investigation into optimising the extraction of limestone (dimension stone Repen) from the Debela Griža quarry. Firstly, this was done by optimising the parameters of a Fantini GU.70-R/XC cutting chainsaw; it was determined that relatively quick Repen cutting can be achieved using the axial force of its blade between 40 N and 75 N. Secondly, a few fractured and unfractured cemented carbide (WC-Co) inserts were metallographically prepared and examined under an optical microscope and SEM with EDS. Etching for the presence of η-phase and Vickers hardness tests were performed on them. Fracture-surface analyses showed that the main reason for insert fracture was hitting harder inclusions in stone. Furthermore, most of the fractured inserts had carbide grains smaller than 2.5 μm, thereby having lower fracture toughness. It was also discovered that samples with a higher binder content and larger carbide sizes exhibited lower Vickers hardness. One of the fractured inserts also contained η-phase, further increasing its susceptibility to fracture.

Keywords: cemented carbide, fracture analysis, stone cutting inserts, chainsaw machine

V pričujočem članku so podani rezultati analize optimiziranja pridobivanja apnenca (Repen) v kamnolomu Debela Griža. V prvem delu so bili optimizirani parametri delovanja samohodne verižne žage Fantini GU.70-R/XC; odkrito je bilo, da je z uporabo aksialne sile med 40 N in 75 N možno doseči relativno hitro rezanje tovrstnega apnenca. V drugem delu je bilo metalografsko pripravljenih in preiskanih nekaj porušenih in neporušenih rezalnih ploščic iz karbidnih trdin (WC-Co). Omenjene preiskave so bile izvedene s svetlobnim mikroskopom in vrstičnim elektronskim mikroskopom z EDS detektorjem. Poleg tega so bile na vzorcih izvedene meritve trdote po Vickersu, vzorci pa so bili na koncu tudi jedkani, namen česar je bilo odkriti potencialno prisotnost faze η v materialu. Z analizo prelomnin je bilo ugotovljeno, da je bila glavni razlog za porušitev rezalnih ploščic prisotnost trših vključkov v rezanem kamnu. Večina karbidov v porušenih ploščicah je imela premer manjši od 2,5 μm, zaradi česar je bila lomna žilavost materiala opazno znižana; odkrito je bilo tudi, da vzorci z višjim deležem veziva in večjimi karbidi izkazujejo nižjo trdoto po Vickersu. V enem izmed porušenih vzorcev je bila dokazana prisotnost faze η, kar je dodatno poslabšalo njegovo odpornost na porušitev.

Ključne besede: karbidna trdina, analiza porušitve, rezalne ploščice za kamen, verižna žaga

1 INTRODUCTION

The use of chainsaws for cutting hard limestone is not new in Slovenia: the first such chainsaws were introduced in the Hotavlje quarry in 1996.[1] In the Debela Griža quarry, where the decorative natural stone Repen is extracted, chainsaws have been used since 2014. Even though these machines are by now not rare in Slovenian quarries, the only research project aimed at providing a better understanding of Slovenian natural-stone extraction with a chainsaw is Ref[1]. In Belgium, in comparison, Mingels[2] and Focant[3] described sawing applications in Belgian red marble, while Boxho,[4] Brych[5] and Neerdael[6] analysed the same for Belgian bluestone. In the past 25 years, relatively few scientific articles have dealt with chainsaw stone cutting, notable exceptions being.[7–10] Despite constant progress in sawing techniques, cutting hard or abrasive stone is still difficult due to low productivity, high consumption of cutting tools and the associated high production costs.

The extraction of Repen in the Debela Griža quarry is carried out using a track-mounted, self-propelling tunnel chainsaw machine Fantini model GU.70-R/XC, shown schematically in **Figure 1**.[11] It is also the world's most common machine for opening and exploring a tunnel cave. Of special importance for the present article is the blade, shown far right in **Figure 1**, where a cutting chain of cemented carbide inserts is located. During stone cutting, this chain is moving around the blade, causing the inserts to penetrate into the stone, while not using any cooling liquid. Usually, there are several inserts at almost the same place on the cutting chain to ensure quicker cutting: the most common variants with 7 and 8 inserts are shown in **Figure 2**.

Stone cutting is the result of the interference between the cutting inserts and the stone at the stone-tool interface. This interference can be described by forces, as shown in **Figure 3**. The most important one, especially for determining the cutting depth of an insert per cut, is the F_n, the axial force of the chainsaw blade. The ideal

*Corresponding author's e-mail:
joze.kortnik@guest.arnes.si (Jože Kortnik)

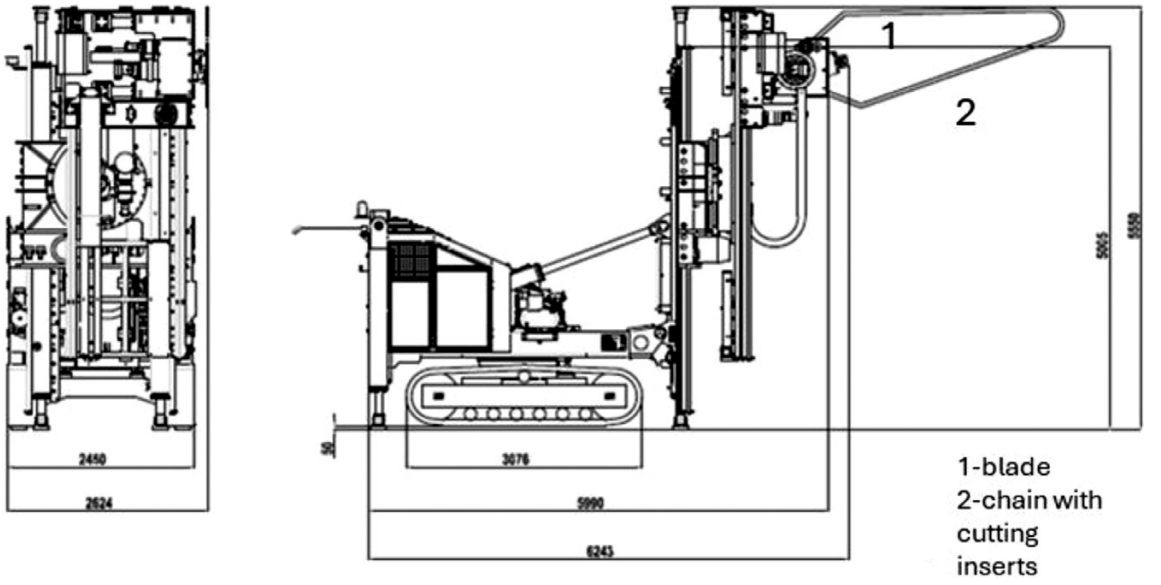

Figure 1: Self-propelled chainsaw machine Fantini GU.70-R/XC[11] with some details denoted in the figure

values of F_n depend on the characteristics of the stone and the machine and can be determined using equations by Purtić.[12]

The axial (thrust) force of the chainsaw arm/blade, Fn, was calculated by equation (1)[18]:

$$F_{\mathrm{n}} = \frac{\sigma_{\mathrm{u}} \cdot l \cdot d \cdot \sin(\alpha + 2\varphi)}{\cos\alpha \cdot \cos^2 \varphi} = k \cdot \sigma_{\mathrm{u}} \cdot l \cdot d \qquad (1)$$

where
σ_{u} (MPa) – compressive strength of the rock
l (m) – length (thickness) of the cutting inserts
d (m) – cutting depth
k (m) – coefficient of friction.

Coefficient of friction:

$$k = \frac{\cos\alpha \cdot \cos^2 \varphi}{\sin(\alpha + 2\varphi)} \qquad (2)$$

The value of the coefficient of friction k is dependent on the angle of the rock internal friction φ and the rake angle α (see **Figure 3**).

Another important factor for determining the efficiency of cutting systems is the specific energy S_{E}: it is defined as the work required to remove one unit volume of stone. Hughes[13] and Mellor[14] have shown that S_{E} can be calculated using equation (3):

$$S_{\mathrm{E}} = \frac{\sigma_{\mathrm{U}}^2}{2E} \qquad (3)$$

where σ_u is the compressive strength of the stone and E the elastic modulus. A comparison between the values of S_{E} and F_n can serve to estimate whether cutting with the calculated F_n would lead to good quality and relatively quick stone cutting.

As mentioned, inserts on the cutting chain are usually made from cemented carbides: these are metal matrix composites, consisting of hard refractory metal carbides

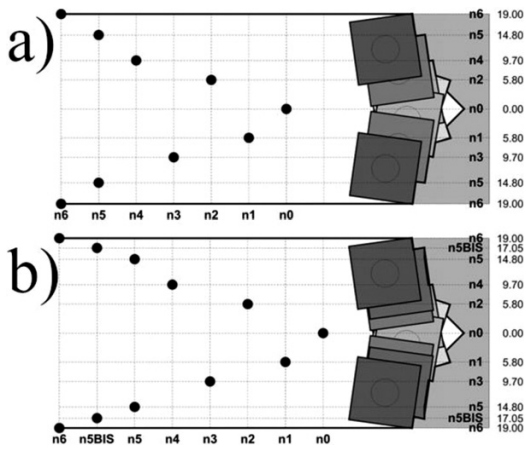

Figure 2: Schematic view of the cutting system with a) 7 (n0….n6) and b) 8 (n0…n6+n5BIS) cutting inserts with their positions on the cutting chain. The n0….n6 numbers coincide and denote the position of the cutting edge of cutting inserts (y-axis) and positions of the cutting insert carriers (x-axis). X-axis has the numbers of cutting inserts carriers, while the y-axis has the distance of the edge of the cutting insert from the central axis (0.00) of the cutting blade

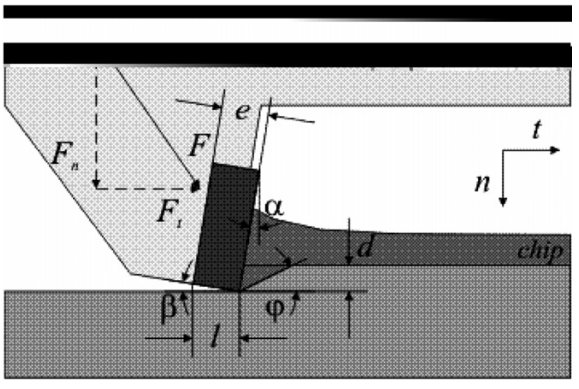

Figure 3: Forces active during chainsaw cutting of stone

embedded in a metal binder matrix.[15,16] The most common example of such material is powder-metallurgy-produced inserts from a powder mixture WC-Co, where the WC phase contributes to the material's wear resistance and hardness, while metallic Co-based solid solution increases the toughness of the material.[16] Such a combination of properties is very desirable, which is why products from these materials are some of the most widespread powder-metallurgy products worldwide, with uses ranging from mining to aerospace to wire drawing.[16,17]

The main goal of the investigation was providing a plan for optimising stone extraction in the Debela Griža quarry. On one hand, this was done by calculating the axial force F_n and proving that using this calculated force, Repen stone could be cut reasonably quickly. On the other hand, the inserts were metallographically examined to demonstrate the influence of their microstructure on the insert properties and to elucidate typical reasons for their fracture. These results could also serve for an optimisation study of the insert microstructure.

2 EXPERIMENTAL WORK

The axial force F_n and specific cutting energy S_E were calculated using equations by Putrić[12] and equation (1), respectively. For these calculations, available data about Repen limestone from Ref.[18] and technical data about the chainsaw from Ref.[11] were used. Furthermore, data from Ref.[11] helped determining the expected cutting depth per insert per cut. All these results were later compared with each other to determine whether cutting with the calculated F_n would lead to good quality and relatively quick stone cutting.

Four Fantini Sandvik H6T stone-cutting inserts or their parts were metallographically examined. One of them was not used at all and will be referred to as sample C. The next two inserts, however, were used and experienced fracture; one of them (labelled P1) fractured relatively close to one of the corners, while the other (P2) fractured approximately in the middle between corners. The last sample (KP) consists of two broken pieces of an insert that were used for studying the fracture surfaces. All the examined samples are shown in **Figure 4**.

Samples C, P1 and P2 were first mounted in resin, ground with a diamond grinding pad and ground further on stone with cubic boron nitride powder of grit sizes P800 and P1200. These samples were then polished using 15-µm, 3-µm and 1-µm diamond pastes. All prepared samples were examined by optical microscopy (OM), often with mostly closed aperture.

All four samples were examined using a Thermo Fisher Quanta 650 scanning electron microscope (SEM) equipped with an Oxford Live EDS Ultim max 40 mm^2 SDD. The latter was mainly used to determine the presence of elements in microstructure phases.

A total of five OM images each for sample C, P1 and P2 at 500× magnification were used to determine the area fraction of binder, which will be used as a measure of binder content throughout the paper. This fraction was estimated using FIJI by adjusting the histogram to select only the binder phase, thus determining its area fraction. An almost identical procedure was performed on four SEM images for each sample; the results of both methods are compared.

The same three samples were also used for low-force Vickers hardness tests measured in HV1 with a loading time of 15 s. At least five measurements were made on each sample at different points on its surface; all measurements were performed in accordance with the ISO 6507-1:2018 standard.[19]

Finally, samples C, P1 and P2 were etched in Murakami's reagent, following a recipe from Ref.[20] The samples were etched for only 2–3 s, which only reveals the possible presence of η-phase in material.[20,21] Hence, etched samples were examined under the OM for the presence of this phase.

3 RESULTS AND DISCUSSION

3.1 Determining the axial force F_n and the cutting depth

Using Putrić's equations, the axial force F_n was calculated to be between 45 N and 70 N for the analysed chainsaw machine. Since the compressive strength σ_u of Repen limestone is known to be approximately 90 MPa,[18] it was possible to determine the cutting depth per insert per cut using data from Ref. [11]. As shown in **Figure 5**, this depth ranges between 0.03 mm and 0.05 mm per cutting insert per cut.

In comparison, the value of specific cutting energy S_E, calculated using equation (1), was approximately 162.7 kJ/m^3. This means that the required S_E can be exceeded between 250 to 430 times by using F_n in the range 40–75 N, thereby ensuring good quality and relatively quick cutting of Repen limestone.

3.2 Investigation of fracture surfaces

Images of the corners of samples C, P1 and P2 in **Figure 6** clearly show that P1 and P2 were used for

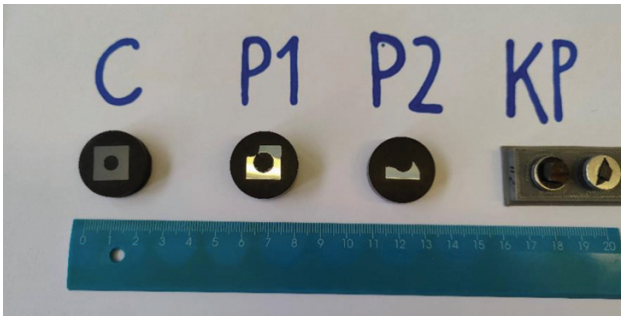

Figure 4: Photograph of analysed samples

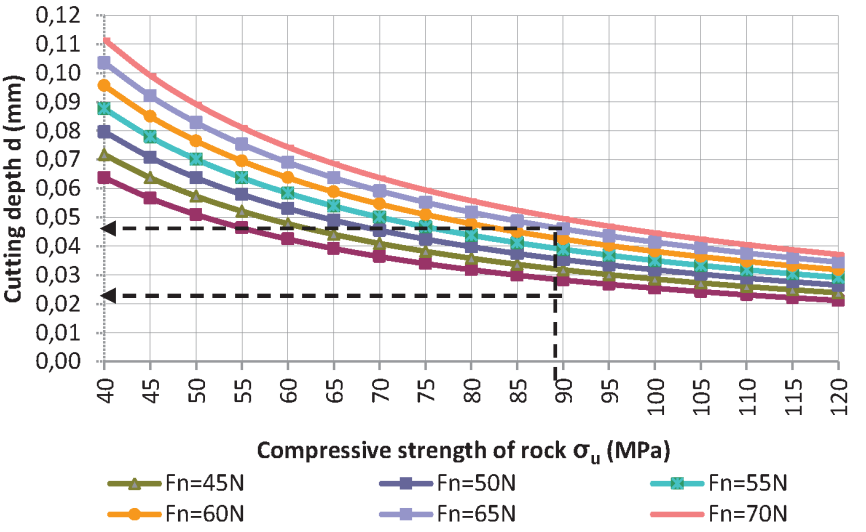

Figure 5: Diagram of the expected insert cutting depth at different compressive strengths of stone σ_u and axial forces of the chainsaw blade F_n.[11]

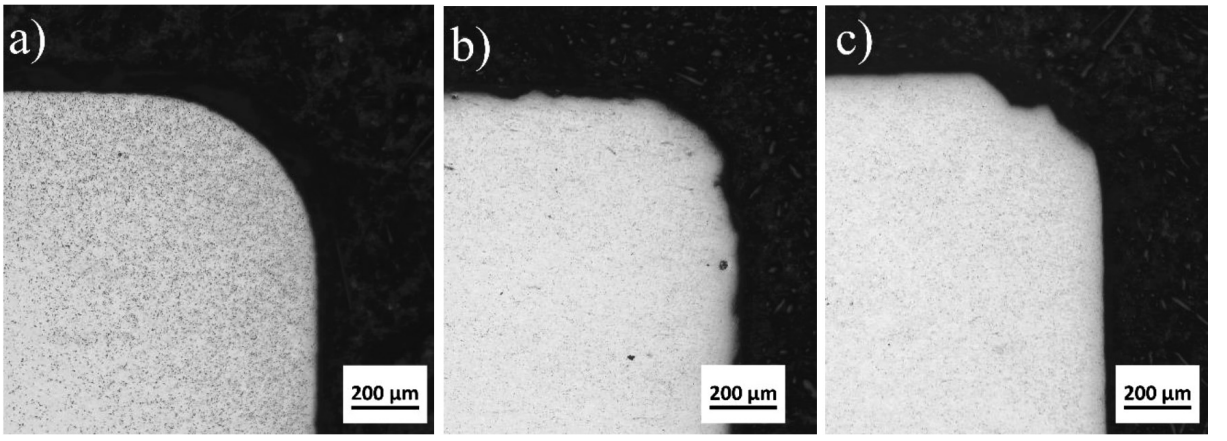

Figure 6: OM images of the corners of samples: a) C, b) P1 and c) P2

stone cutting, as their corners show signs of wear. In comparison, insert C has almost perfectly rounded corners, confirming it has been unused.

Samples P1 and P2 exhibit fracture surfaces; in P1, these are close to one of the corners (**Figure 4**), suggesting that the fracture was at least partially caused by a sudden spike in internal stress. These spikes were probably caused by sudden increases in reaction forces, when the inserts hit inclusions of harder material in the stone. Some spikes of internal stress were probably high enough to break a small portion of the material.

In comparison, the fracture in P2 occurred roughly midway between two corners. A closer metallographic examination revealed that one of the surfaces has a distinct fracture surface (**Figure 7**) on the inner surface of the insert, with a sharp-edged fracture and several cracks propagating into the material. It is probable that this is exactly where a crack initiated, having led to insert fracture.

Moreover, only in this area another material is adhered to the fracture surface. According to EDS this material contains 97.36 weight % Fe, 1.26 % Cr, 0.85 % Mn and 0.53 % W; therefore, this is likely steel from the screw, used to attach the inserts to the saw chain. Said steel adhered to the surface due to the wear of the screw, which was either a result of a newly formed edge in ce-

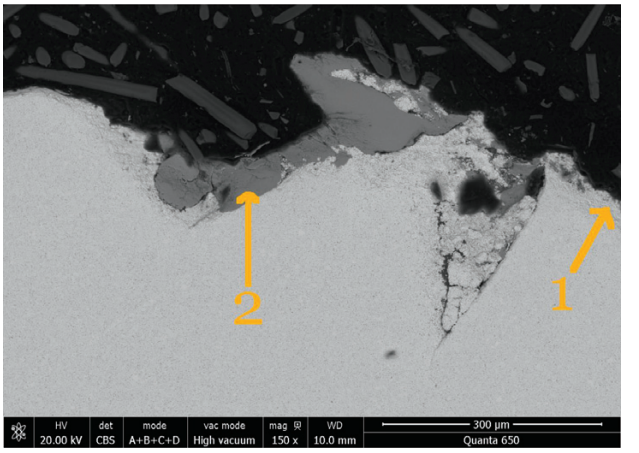

Figure 7: SEM (BSE) image of a distinct fracture surface on sample P2. Number 1 marks the inner surface of the insert and 2 the material of the steel screw, adhered to the fracture surface

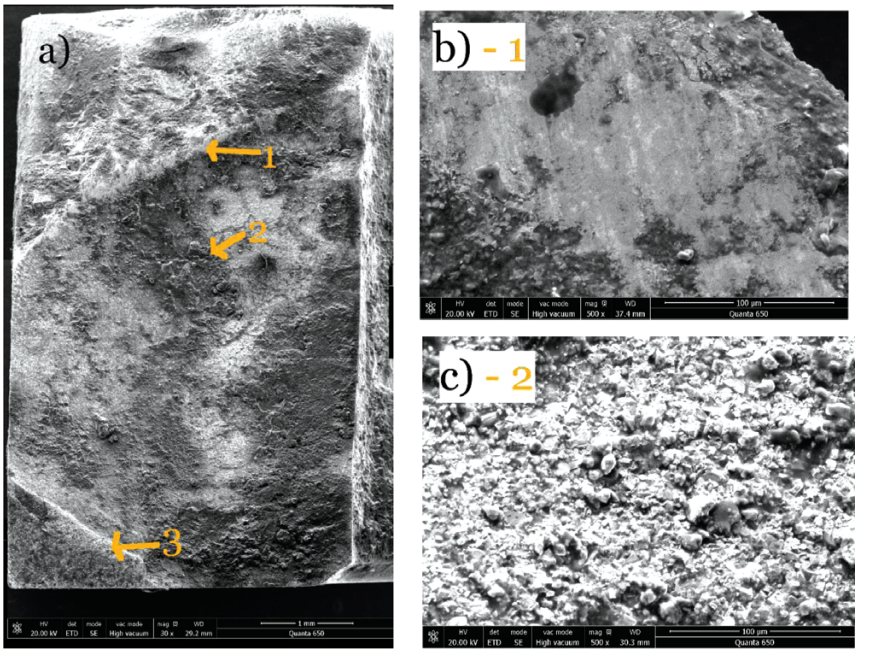

Figure 8: a) SEM (SE) image of the entire fracture surface of KP sample. Number 1 marks the site of transgranular fracture, 2 intergranular fracture and 3 a large ledge, b) SEM (SE) image at higher magnification of transgranular fracture on another analysed sample; the surface is almost identical to the one, found on site 1 in a), c) SEM (SE) image at higher magnification of intergranular fracture on site 2 in a).

mented carbide or a consequence of the eccentricity of the axis of rotation. It is noteworthy that this adhered steel is not present in the cracks, suggesting they were formed at a later stage of fracture.

SEM images of the fracture surface on sample KP can be seen in **Figure 8**. The fracture propagated from the upper part with a "ridge" of white, relatively smooth fracture surface, labelled 1 in **Figure 8a**; an almost identical surface can be seen at higher magnification in **Figure 8b**. The smoothness of this part indicates that the fracture was locally transgranular, most likely caused by a sudden increase in internal stress. Above the mentioned "ridge" the fracture surface belongs to a different fracture plane.

Most of the remaining surface exhibits intergranular fracture, which means that a crack propagated along grain boundaries between carbides and through binder.[22,23] This can be clearly seen in **Figure 8a** and **8c** due to a very uneven surface. Some of the carbides obviously protrude from the surface plane.[22] Visually, this part of the fracture surface looks very similar to that observed and described in detail in Ref.[22]

At the lower end of **Figure 8a** a rather large ledge, labelled 3, is clearly visible. It probably formed when the cracks propagated to such an extent that the material in the inserts could no longer withstand the external forces, causing the inserts to fracture.

3.3 Phases in samples and their approximate compositions

In the microstructure images in **Figure 9**, two phases are immediately recognisable: sharp-edged carbides, surrounded by the binder phase. Using EDS, it was confirmed that the binder phase consists almost exclusively of cobalt, while the carbides consist of tungsten and carbon.

OM analysis after etching revealed that samples C and P1 contain no visible η-phase. In P2, however, this phase can be found, as shown in **Figure 10**. Its distribution across the sample is very uneven, with large areas in

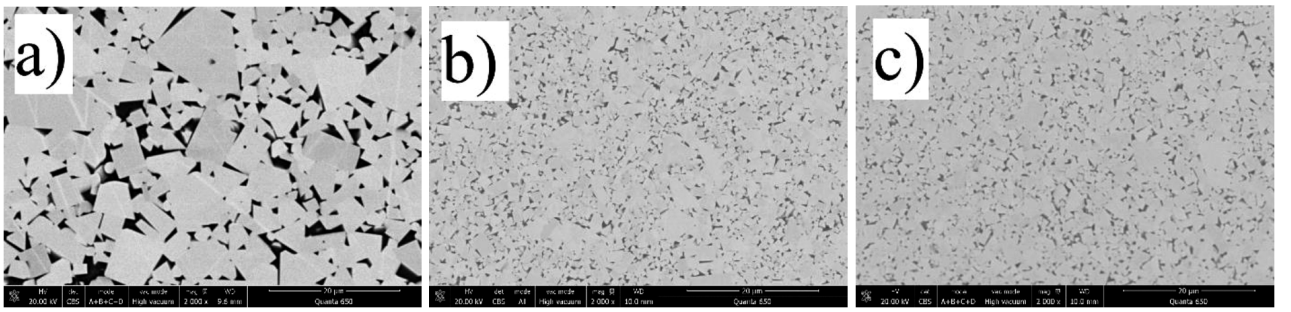

Figure 9: SEM (BSE) images of analysed samples: a) C, b) P1 and c) P2

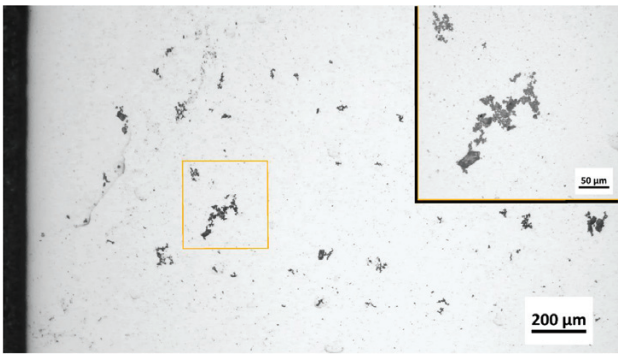

Figure 10: Combined OM images of P2 after etching 3 s with Murakami's reagent. Both orange rectangles show the same area. The dark phase is mostly η.

the centre being completely without it, while there is much more of it closer to the edges. η-phase is formed due to a local deficit of carbon, resulting in dissolution of tungsten carbide into liquid cobalt; this deficit could be a result of decarburisation, which is more pronounced closer to the edges.[17,20] It is likely that decarburisation took place during sintering or when hot green parts of initial η-phase were exposed to the atmosphere.[17]

In cemented carbides, the presence of η-phase is generally undesirable, as its brittle nature lowers the fracture toughness of the material.[17,20] This is particularly pronounced when its morphology is dendrite-like, as is the case for sample P2.[17] Therefore, it is likely that the presence of η-phase in P2 contributed to its susceptibility to fracture.

3.4 Binder content and hardness measurement results

The results of the binder-content measurements are shown in **Table 1**. Sample C contains the highest area fraction of binder, while this fraction is only slightly higher in P2 compared to P1. The exact fractions differ slightly between those determined from the OM and SEM images. On the one hand, the OM images show lower contrast and more surface artefacts due to the unevenness of the examined surface. This unevenness was caused by grinding and polishing: as the binder phase is much less wear-resistant, more of it was ground off. Consequently, the surfaces examined may not contain the same surface fraction of binder as would be observed on an undeformed surface.

On the other hand, SEM images were taken with an electron acceleration voltage of 20 kV, which means that some of the backscattered electrons penetrated relatively deeply into the material, especially into the binder, since cobalt has a much lower atomic number than tungsten. As a result, some carbide surfaces that "descend" inside the sample can be seen on the SEM images, see for example **Figure 9**. Therefore, the binder content results obtained from SEM images may also not be entirely accurate.

A difference between the binder area fractions of the samples can be seen with the naked eye when comparing the SEM images of their microstructures. For example, **Figure 9**, shows a comparison of these microstructures at 2000× magnification.

It is known that a higher binder content increases the quasi-static fracture toughness,[22,24] but also the fatigue susceptibility.[24,25] The latter has been partly explained by a strain-induced phase transformation of cobalt from a metastable *fcc* to *hcp* structure, which causes embrittlement of the binder due to facilitated crack propagation in the *hcp* structure and along its stacking faults.[25,26] Indeed the slopes of the Wöhler curves have been found to increase with higher binder content,[27] confirming why cemented carbides with relatively low binder content are used in rock-drilling bits, for example.[28]

However, the differences in fatigue susceptibility of cemented carbides with only slightly different binder content are relatively small.[22,26] For example, in Ref.[22], the difference in dynamic fracture resistance between specimens with 6 and 13 % binder surface fraction was within experimental error.[22] Consequently, it seems unlikely that a slightly higher binder content in C could have contributed to a faster deterioration of properties under dynamic loading.

On the other hand, the influence of binder content on the overall hardness of the material is much more pronounced.[24] A higher binder content generally reduces the hardness of the material, as the hardness of the binder is lower than the hardness of the carbides.[24]

Another important factor that determines the mechanical properties of cemented carbides, including Vickers hardness, is the grain size of the carbides. A comparison of the images in **Figure 9** shows that C contains significantly coarser grains on average than P1 and P2. The average grain sizes of P1 and P2 appear to be relatively

Table 1: Measured binder content in analysed samples

Sample	C		P1		P2	
Phase	(Co) (binder) [%]	WC (carbides) [%]	(Co) (binder) [%]	WC (carbides) [%]	(Co) (binder) [%]	WC (carbides) [%]
Average area fraction of phase, determined using LOM images	10.2	89.8	7.8	92.2	9.0	91.0
Standard deviation	0,50		0,18		0,76	
Average area fraction of phase, determined using SEM images	11.2	88.8	9.4	90.6	9.7	90.8
Standard deviation	1.33		0.30		0.19	

similar, but P1 appears to contain more of the smallest visible carbides. The literature states that smaller carbides in cemented carbides increase the overall hardness of the material, but also reduce its fracture toughness.[22,24,28] The latter has been explained by the fact that intergranular cracks must take a longer and more tortuous path when the carbides are larger.[22,29]

The difference in observed carbide grain sizes between the samples analysed is probably the main reason why P1 and P2 were more susceptible to fracture than C. In fact, coarse-grained grades of cemented carbide are used in most drilling bits for rock mining, which according to the classification of the Facherband Pulvermetallurgie association means that these grains have a diameter of at least 2.5 μm.[17,28] While grains of this size make up the majority of carbide grains in C, most of the grains in P1 and P2 have a diameter smaller than 2.5 μm.

Table 2: Results of Vickers hardness measurements.

Sample	C	P1	P2
Average Vickers hardness [HV1] values	1243	1568	1502
Standard deviation	32.2	19.1	45.1

The results of the Vickers hardness measurements shown in **Table 2** are in good agreement with the previously mentioned influences of the binder content and carbide grain sizes of the analysed samples, as can be found in the literature.[17,22,24] Sample C with the largest grains and the highest binder content has the lowest hardness, while P1 with the smallest grains and the lowest binder content has the highest hardness.

4 CONCLUSIONS

Based on the analysis of Repen stone's cutting parameters and a metallographic examination of cutting inserts, the following can be concluded:

Good-quality and relatively quick Repen stone cutting can be achieved using the Fantini GU.70-R/XC chainsaw machine, when the axial force of its blade F_n is in the range of 40–75 N.

The used inserts most likely fractured due to sudden spikes of internal stress when the chainsaw hit harder inclusions in the stone. Most of the fracture surfaces show an intergranular fracture.

One of the samples contains η-phase, which increased its susceptibility to fracture.

Samples with a higher binder content and larger carbide sizes exhibit a lower Vickers hardness.

The measured size of most of the carbide grains in fractured samples were smaller than 25 μm. This is usually related to a lower fracture toughness of the inserts even though no fracture toughness measurements were made during this work. For the purpose of dry cutting of limestone a combination of large (<5 μm) and small (>5 μm) WC particles appears to be the best choice, giving the cutting inserts a suitable combination of edge and bulk toughness.

Acknowledgement

The authors would like to express their gratitude to Kamnoseštvo Tavčar d. o. o. for providing the analysed inserts, data regarding the chainsaw machine and for their voluntary work.

5 REFERENCES

[1] J. Kortnik, B. Markoli, Dry-cutting options with a chainsaw at the Hotavlje I natural-stone quarry, Mater. Tehnol., 49 (**2015**) 1, 103–110
[2] C. Mingels, Utilisation d'une haveuse Perrier dans une carriere de marbre, Ann. Mines Belg., 2 (**1971**) 1, 121–130
[3] J. Focant, Utilisation des haveuses Perrier dans I'exploitation des carrieres de Marbres Rouge, Ann. Mines Belg., 9 (**1977**) 2, 819–823
[4] J. Boxho, Essai d'una haveuse Perrier dans le Petit Granit, Ann. Mines Belg., 2 (**1971**) 3, 131–142
[5] J. Brych, Les outils autoaffutants au service du havage des roches dures, Ann. Mines Belg., 2 (**1975**) 1, 165–180
[6] B. Neerdael, Contribution ill'etude de la destructibilite des roches dures telles que les callcaires crino'idiques de Soignies, Faculte Polytechnique de Mons, Travail de fin d'etudes, 1975, 5–18
[7] F. I. Dagrain, Understanding stone cutting mechanisms for the design of new cutting tools sequences and the cutting optimization of chain saw machines in Belgian blue stone quarries, Diamante, Aplicazioni & Technologia, 17 (**2011**) 66, 55–67
[8] S. Turchetta, L. Carrino, W. Polini, CVD diamond insert in stone cutting, Diamond Relat. Mater., 14 (**2005**) 3–7, 641–645, doi:10.1016/j.diamond.2004.10.031
[9] H. K. Tonshoff, H. Hillmann-Apman, J. Asce, Diamond tools in stone and civil engineering industry: cutting principles, wear and application, Diamond Relat. Mater., 11 (**2002**) 3–6, 736–741, doi:10.1016/S0925-9635(01)00561-1
[10] Y. Li, H. Huang, J. Y. Shen, X. P. Xu, Y. S. Gao, Cost-effective machining of granite by reducing tribological interactions, J. Mater. Process. Technol., 129 (**2002**) 1–3, 389–394, doi:10.1016/S0924-0136(02)00699-4
[11] Fantini GU70-R-XC Technical Paper, https://www.fantinispa.it/wp-content/uploads/2015/05/brochure-gu.pdf, 11. 12. 2024
[12] N. Purtić, Drilling and Blasting/Bušenje i miniranje, Rudarsko-geološki fakultet, Beograd 1991, 20–22
[13] H. Hughes, Some aspects of rock machining, Int. J. Rock Mech. Min. Sci., 9 (**1972**) 2, 205–211
[14] M. Mellor, Normalization of specific energy values, Int. J. Rock Mech. Min. Sci., 9 (**1972**) 5, 661–663
[15] T. Kresse, D. Meinhard, T. Bernthaler, G. Schneider, Hardness of WC-Co hard metals: Preparation, quantitative microstructure analysis, structure-property relationship and modelling, Int. J. Refract. Met. Hard Mater., 75 (**2018**), 287-293, doi:10.1016/j.ijrmhm.2018.05.003
[16] C. Chen, B. Huang, Z. Liu, Y. Li, D. Zou, T. Liu, Y. Chang, L. Chen, Additive manufacturing of WC-Co cemented carbides: Process, microstructure, and mechanical properties, Addit. Manuf., 63 (2023), doi:10.1016/j.addma.2023.103410
[17] J. García, V. Collado Ciprés, A. Blomqvist, B. Kaplan, Cemented carbide microstructures: a review, Int. J. Refract. Met. Hard Mater., 80 (**2019**), 40–68, doi:10.1016/j.ijrmhm.2018.12.004
[18] Natural stone "Repen" geotechnical report /Poročilo o priskavi naravnega kamna – preiskave nekaterih fizikalno-mehanskih lastnosti vzorcev P-1 in P-2, ZRMK, Ljubljana 1993, 15
[19] ISO 6507-1:2018(E) Metallic materials, Vickers hardness test, Part 1: Test method, ISO Committee, Geneve

[20] G. Petzow, Metallographisches, keramographisches, plastographisches Ätzen, 6. vollst. überarb. Aufl., Gebrüder Borntraeger, Berlin – Stuttgart 1994, 219

[21] M. N. Haller, Cemented Carbides: Metallographic Techniques and Microstructures. In: J. W. Pridgeon (ed.), ASM Handbook Vol. 9. Metallography and Microstructures, Eight printing, ASM International, Materials Park, Ohio, 1998, 514–528

[22] P. Jewell, L. Shannahan, S. Pagano, R. DeMott, M. Taheri, L. Lamberson, Rate and microstructure influence on the fracture behavior of cemented carbides WC-Co and WC-Ni, Int. J. Fract., 208 (**2017**), 203–219, doi:10.1007/s10704-017-0237-8

[23] K. Mandel, M. Radajewski, L. Krüger, Strain-rate dependence of the compressive strength of WC–Co hard metals, Mater. Sci. Eng., A, 612 (**2014**), 115–122, doi:10.1016/j.msea.2014.06.020

[24] J. J. Pittari, J. J. Swab, J. Wright, K. Atwater, Mechanical evaluation of WC-Co materials with varying microstructures, International Journal of Refractory Metals and Hard Materials, 104 (**2022**), doi:10.1016/j.ijrmhm.2022.105809

[25] J.M. Tarragó, J.J. Roa, V. Valle, J. M. Marshall, L. Llanes, Fracture and fatigue behavior of WC–Co and WC–CoNi cemented carbides, Int. J. Refract. Met. Hard Mater., 49 (**2015**), 184-191, doi:10.1016/j.ijrmhm.2014.07.027

[26] S. Kursawe, Ph. Pott, H. G. Sockel, W. Heinrich, M. Wolf, On the influence of binder content and binder composition on the mechanical properties of hardmetals, Int. J. Refract. Met. Hard Mater., 19 (**2001**) 4–6, 335–340, doi: 10.1016/S0263-4368(01)00026-9

[27] T. Sailer, M. Herr, H.-G. Sockel, R. Schulte, H. Feld, L.J. Prakash, Microstructure and mechanical properties of ultrafine-grained hardmetals, Int. J. Refract. Met. Hard Mater., 19 (**2001**) 4–6, 553–559, doi: 10.1016/S0263-4368(01)00041-5

[28] Y. Torres, J.M. Tarrago, D. Coureaux, E. Tarrés, B. Roebuck, P. Chan, M. James, B. Liang, M. Tillman, R.K. Viswanadham, K.P. Mingard, A. Mestra, L. Llanes, Fracture and fatigue of rock bit cemented carbides: Mechanics and mechanisms of crack growth resistance under monotonic and cyclic loading, Int. J. Refract. Met. Hard Mater., 45 (**2014**), 179–188, doi:10.1016/j.ijrmhm.2014.04.010

[29] A. Belenky, I. Bar-On, D. Rittel, Static and dynamic fracture of transparent nanograined alumina, J. Mech. Phys. Solids, 58 (**2010**) 4, 484–501, doi:10.1016/j.jmps.2010.02.002